Contents lists available at ScienceDirect

Carbohydrate Polymers

journal homepage: www.elsevier.com/locate/carbpol





A novel structural design of cellulose-based conductive composite fibers for wearable e-textiles

Wangcheng Liu^{a,*}, Hang Liu^{a,b,**}, Zihui Zhao^b, Dan Liang^b, Wei-Hong Zhong^c, Jinwen Zhang^a

- ^a Composite Materials and Engineering Center, Washington State University, Pullman, WA 99164, USA
- ^b Apparel, Merchandising, Design and Textiles, Washington State University, Pullman, WA 99164, USA
- ^c School of Mechanical and Materials Engineering, Washington State University, Pullman, WA 99164, USA

ARTICLE INFO

Keywords: Regenerated cellulose fibers Multi-phase composites E-textiles Electrical conductivity Eco-friendly processing Polyaniline

ABSTRACT

Cellulose-based conductive composite fibers hold great promise in smart wearable applications, given cellulose's desirable properties for textiles. Blending conductive fillers with cellulose is the most common means of fiber production. Incorporating a high content of conductive fillers is demanded to achieve desirable conductivity. However, a high filler load deteriorates the processability and mechanical properties of the fibers. Here, developing wet-spun cellulose-based fibers with a unique side-by-side (SBS) structure via sustainable processing is reported. Sustainable sources (cotton linter and post-consumer cotton waste) and a biocompatible intrinsically conductive polymer (i.e., polyaniline, PANI) were engineered into fibers containing two co-continuous phases arranged side-by-side. One phase was neat cellulose serving as the substrate and providing good mechanical properties; another phase was a PANI-rich cellulose blend (50 wt%) affording electrical conductivity. Additionally, an eco-friendly LiOH/urea solvent system was adopted for the fiber spinning process. With the proper control of processing parameters, the SBS fibers demonstrated high conductivity and improved mechanical properties compared to single-phase cellulose and PANI blended fibers. The SBS fibers demonstrated great potential for wearable e-textile applications.

1. Introduction

E-textiles are electrical or electronic textile products that can display versatile functionalities, such as transmitting electronic signals, converting or storing energy, sensing and adapting their properties in response to environmental stimuli originated from changes in electricity, humidity, light, temperature, pH, magnet, or tactile deformation (Castano & Flatau, 2014; Hu, Meng, Li, & Ibekwe, 2012; Mirabedini, Foroughi, & Wallace, 2016; Shi et al., 2019; Stoppa & Chiolerio, 2014; Yang, Xie, Li, & Zhu, 2017). *E*-textiles have garnered significant interest for applications in the fields of medicine, personal health, and sportswear, representing a crucial research direction in the revolution of nextgeneration materials (Grancarić et al., 2018; Patel, Park, Bonato, Chan, & Rodgers, 2012; Stoppa & Chiolerio, 2014; Zeng et al., 2014).

Due to its great mechanical properties, availability, sustainability, flexibility, and comfort, cellulose is an ideal material for fabricating multi-functional textiles. For cellulosic composite conductive fibers, conductive fillers need to be incorporated into fibers. Among the fillers

used, carbon nanotubes, carbon nanofibers, graphene, and carbon blacks are commonly adopted. Usually, carbon nanofillers are mixed with cellulose in a solvent to form a solution, which then undergoes wetspinning or electrospinning. Those fibers can have conductivities between 10⁻⁴ and 10² S/cm depending on the filler load and processing parameters (Härdelin & Hagström, 2015; Kim, Park, Kim, & Park, 2010; Liu, Wang, et al., 2019; Lu, Zhang, Jian, Shao, & Hu, 2012; Ma et al., 2021; Mahmoudian, Reza Sazegar, Afshari, & Uzir Wahit, 2017; Qi et al., 2015; Rahatekar et al., 2009; Zhang et al., 2007). However, the safety of carbon nanofillers is debatable in respect of both processing (e.g., aqueous pollution and inhalation hazards) and end-product application in wearables (e.g., cytotoxicity and skin irritation) (Jia et al., 2005; Shi et al., 2020; Sousa et al., 2020; Wick et al., 2007; Yang, Li, Tan, Peng, & Liu, 2013). With this consideration, intrinsically conductive polymers (ICP) can be a favorable alternative for wearable applications (Balint, Cassidy, & Cartmell, 2014; Guo & Ma, 2018; He et al., 2019; Ismar, Kurşun Bahadir, Kalaoglu, & Koncar, 2020). Polyaniline (PANI), one representative ICP, has the advantages of easy synthesis, great

^{*} Corresponding author.

^{**} Correspondence to: H. Liu, Apparel, Merchandising, Design and Textiles, Washington State University, Pullman, WA 99164, USA. *E-mail addresses*: wangcheng.liu@wsu.edu (W. Liu), hangliu@wsu.edu (H. Liu).

biocompatibility, low cost, and tunable conductivity responding to environmental changes (e.g., pH, humidity, and redox reaction). Therefore, PANI fibers can inherently function as chemical or biological sensors (Bavatharani et al., 2021; Bhadra, Khastgir, Singha, & Lee, 2009; Ćirić-Marjanović, 2013; Lai et al., 2016; Liu, Zhong, Liu, Zhang, & Liu, 2020; Sen, Mishra, & Shimpi, 2016; Tanguy, Thompson, & Yan, 2018).

Cellulose-based fiber spinning is solution based. Only a few solvent systems can dissolve cellulose, and some are toxic and environmentally hazardous, such as cuprammonium solution and carbon disulfide (CS2) (Rose & Palkovits, 2011; Sayyed, Deshmukh, & Pinjari, 2019; Wang, Lu, & Zhang, 2016). In contrast, alkali/urea mixtures (i.e., LiOH/urea/ water or NaOH/urea/water) offers a more sustainable, safer, and economical alternative (Cai & Zhang, 2005, 2006; Cai et al., 2004; Chen et al., 2007; Li et al., 2010; Liu, Liu, et al., 2019; Mao, Zhang, Cai, Zhou, & Kondo, 2008; Qi, Chang, & Zhang, 2008). In the dissolving process using this solvent mixture, alkalis adhere to the hydroxyl groups of cellulose, forming new hydrogen bonds and breaking the cellulose intermolecular hydrogen bond networks at low temperatures. Meanwhile, urea interacts with the alkali ions to form inclusion complexes that promote the penetration of alkali hydrates into cellulose macromolecules and stabilizes the solutions. In the subsequent fiber spinning process, the dope solutions are coagulated with acidic aqueous nonsolvents, regenerating cellulose fibers. All the applied bases and acids are readily available in the industry and can be neutralized into lowhazardous inorganic salts for further distillation to minimize the negative environmental impact (Chen et al., 2015; Li, Wang, Lu, & Zhang, 2015; Qiu et al., 2018; Tu et al., 2020; Vehviläinen et al., 2008; Xie et al., 2021; Yang, Zhang, Lang, & Yu, 2018; Zhang, Li, Yu, & Hsieh, 2010; Zhu et al., 2018).

In this study, developing cellulose/PANI conductive composite fibers for wearable e-textiles via the eco-friendly alkali/urea method is reported. To further highlight the sustainable nature of this process, cotton linter (CL) and waste cotton t-shirts (CS), representing pre-consumer and post-consumer textile waste, were utilized to form the matrix of the composite fibers. Preliminary studies showed that the percolation threshold for cellulose/PANI blend fibers to be conductive was at least 33 wt%. With this high filler load, the mechanical properties of blend fibers severely deteriorated. Therefore, we modified the traditional wetspinning technique to engineer the composite fibers with a heterogeneous structure of two co-continuous phases arranged side-by-side (SBS). One phase was a conductive cellulose/PANI blend with a high PANI load (50 wt%), and the other phase was neat cellulose. The hypothesis was that, with proper processing, the two phases would have strong interfacial bonding, so the neat cellulose served as the substrate to support the PANI-rich phase, producing fibers with both high conductivity and excellent mechanical performance. The relationships between process, structure, and property, as well as the effectiveness of the SBS structural design on composite fibers, were investigated and discussed.

2. Experiments

2.1. Materials

Polyaniline (PANI, MW = 50,000 g/mol), p-toluenesulfonic acid monohydrate (pTSA \bullet H₂O, assay = 98.5 %), citric acid (CA), and bis (ethylenediamine) copper(II) hydroxide solution (1 M in water) were purchased from Sigma-Aldrich. Lithium hydroxyl monohydride (LiOH \bullet H₂O, assay = 99.0 %), urea (assay = 100.0 %), and ammonium sulfate ((NH₄)₂SO₄, assay = 98.0 %) were acquired from Alfa-Aesar. Sulfuric acid (H₂SO₄, assay = 95.0–98.0 %) was purchased from Fisher Scientific. All chemical agents were used as received. Low-micronaire cotton linter (CL) was kindly provided by Cotton Incorporated. Blue fibers were from a shredded cotton t-shirt (CS).

2.2. Preparation of dope solutions

Cotton fibers with a high degree of polymerization (DP) were hydrolyzed by acid for better solubility, following the procedures in our previous work (Liu, Liu, et al., 2019). Briefly, cotton fibers were immersed in 0.05 wt% $\rm H_2SO_4$ solution and treated under 120 °C for 12 min with an autoclave. The DP of treated and untreated fibers was then determined following the ASTM D1795 standard. Raw cotton linter (coded CL-1), hydrolyzed cotton linter (coded CL-2), and hydrolyzed cotton t-shirt (coded CS) fibers with DP of 1080, 710, and 370, were utilized to prepare solutions for fiber spinning. Since the raw cotton t-shirt fibers had a DP of over 1800, without hydrolyzing, it was difficult to dissolve at a concentration that was high enough for fiber spinning.

Before dissolving, cotton fibers were dried in a conventional oven and then sealed in a freezer ($-12\,^{\circ}$ C). The LiOH/Urea/H₂O solvent (4.6/15/80.4 wt%) was prepared and pre-cooled to $-12.5\,^{\circ}$ C. After that, cotton fibers were added into the alkali solvent under vigorous stirring (1000 rpm) for 15 min. Cotton concentrations of 1.5 wt% for CL-1, 3 wt% for CL-2, and 6 wt% for CS were adopted in order to obtain solutions with proper viscosities for fiber spinning.

The cellulose/PANI blend solutions were prepared in two sequential steps. Initially, PANI particles (6 wt%) were dispersed into DI water by intermittent ultrasonication (Branson SSE-1) under 25 % amplitude for 20 min (\sim 5 °C). Then, the pure PANI dispersion was homogenized with the neat cellulose solution in a weight ratio of 1:3. To obtain the same cotton concentration in the blend solution as their respective neat solution, the cotton concentrations of the neat solution used to blend with PANI were 2 wt%, 4 wt%, and 8 wt% for CL-1, CL-2, and CS, respectively. The homogenization was conducted with a high-speed mixer (Cole-Parmer Model 50006-01) at 2500 rpm for 15 min (5 °C). A summary of the dope solutions is listed in Table 1.

2.3. Wet-spinning process

For spinning, the solution was transferred to a 12 mL syringe (Covidien Monojet) and loaded on a syringe pump (New Era NE 1010). The wet-spinning process was carried out in two settings using the same processing parameters but different spinneret configurations: (a) traditional monojet spinning: the use of an 18 gauge blunt needle capped with a plastic conical tip (diameter = 365 μm) to extrude one dope solution (8 mL/h) for homogenous fibers; and (b) "side-by-side (SBS)" spinning: the use of a core-sheath eccentric needle (18–23 gauges) capped by the same conical tip to extrude one neat cotton solution and one cotton/PANI blend solution (6–2 mL/h) at the same time for SBS heterogeneous fibers as demonstrated in Fig. S1. Fibers produced were conditioned at 21 °C and 45 % relative humidity (RH) for at least 3 days before characterization.

2.4. Characterization

2.4.1. Solution rheology

Rheology testing of dope solutions was performed on an oscillatory rheometer (TA instrument, DHR-2) equipped with 25 mm parallel plates at 20 $^{\circ}$ C. The steady shear viscosity of dope solutions was measured and

Table 1Dope solution compositions.

| Type of cotton fibers | Codename of solution | Composition of cellulose/PANI (by weight) | PANI load in the whole fiber (wt%) |
|-----------------------|----------------------|---|--|
| Raw cotton linter | CL-1 Neat | 1.5/0 | 0 |
| (DP = 1080) | CL-1 Blend | 1.5/1.5 | 50 |
| Hydrolyzed cotton | CL-2 Neat | 3/0 | 0 |
| linter (DP $= 710$) | CL-2 Blend | 3/1.5 | 33 |
| Hydrolyzed blue t- | CS Neat | 6/0 | 0 |
| shirt ($DP = 370$) | CS Blend | 6/1.5 | 20 |

recorded as a function of different shear rates (1–1000 s^{-1}). The gap distance of the parallel plates was 500 μm . The testing result was based on the average of 3 replicates.

2.4.2. Linear density and tensile properties

Tensile testing of single fibers was performed on a universal testing machine (Instron 5565) equipped with a 100 N load cell following the ASTM D3822 standard. The grip distance was 25 mm, and the crosshead speed was maintained at 10 mm/min (40 % strain rate per min). The testing was conducted at 21 °C and 45 % RH. Mean and standard deviations of tensile tenacity and elongation at break were measured from the results of 20 replicates. To calculate the tenacity, the linear density ($T_{\rm d}$) of single fibers was determined by following the ASTM D1577 standard, and the fiber cross-section area was calculated following Eq. (1) (Liu, Chang, Zhang, & Liu, 2022):

$$A = \frac{T_d}{10^4 \times d} \tag{1}$$

where d is the theoretical density of the fibers calculated based on the composition and density of cellulose and PANI (cellulose = 1.55 g/cm^3 ; PANI = 1.245 g/cm^3).

2.4.3. Morphology

The longitudinal and cross-sectional morphology of fibers were examined using a field emission scanning electron microscope (FE SEM, Quanta 200F) and a digital optical microscope (Keyence VHX-7000). The cross-section samples were prepared by immersing the fiber samples in liquid nitrogen for 30 min and then fractured. For SEM, all samples were sputter-coated with 15 nm gold (Technics Hummer V). An electron field of 30 kV was used for imaging. The average fiber diameter was determined using 30 randomly selected fibers from surface images obtained by the optical microscope.

2.4.4. Electrical conductivity

The resistivity of fibers was determined by an electrometer (Keithley 6517B) on the two-probe testing mode (100 V) with direct current (DC). Single fibers of 2 cm were mounted onto the testing frame with conductive adhesive tapes. The two ends of the fibers were coated with conductive ink (Bare Conductive) to ensure good contact with the tape and served as the two electrodes. The conductivity of a single fiber (δ) was calculated by Pouillet's law, where the area was derived from Eq.

(1).

3. Results and discussion

3.1. Fibers prepared by the traditional monojet spinning

Six solutions were prepared based on the compositions in Table 1 and spun into fibers using a monojet nozzle. Solution images and their viscosity are shown in Fig. S2. PANI was evenly mixed in the cellulose solution, although some large aggregates of approximately 10 um could be seen. Observed from SEM images (Fig. 1), the cellulose/PANI blend fibers displayed a rough surface due to the PANI aggregates, contrasting with the smooth surface of the neat cellulose fibers. As shown in Table 2, the blend fibers had a tensile strength of 0.17 cN/dtex, 0.51 cN/dtex, and 0.59 cN/dtex, dropped from 0.83 cN/dtex, 0.73 cN/dtex, and 0.68 cN/dtex of the neat cellulose fibers for the CL-1 blend, CL-2 blend, and CS blend, respectively. The higher the PANI concentration, the larger the tensile strength drop. In terms of electrical conductivity, all these neat and blend fibers, except for the CL-1 Blend, were insulating with conductivity at or lower than 10^{-8} S/cm. CL-1 Blend with 50 % of PANI had a conductivity of 0.68–1.5 \times 10⁻². Since the conductivity of PANI strongly depended on acid doping, an additional doping step was carried out by immersing the fibers in a 10 % pTSA/water solution for 24 h in order to check whether the low conductivity was due to insufficient doping in the coagulation bath during fiber production. Results (Table S1) showed that redoping increased the conductivity of the CL-1 blend only by 5-10 times but not the CL-2 blend and CS blend. This indicated that the percolation threshold of PANI in cellulose is larger than 33 %. This result was consistent with what others reported (Kim, Hobbs, Wang, Rutten, & Wamser, 2009; Low et al., 2014; Low et al., 2015; Norris, Shaker, Ko, & MacDiarmid, 2000; Ucar, Kizildag, Onen, Karacan, & Eren, 2015).

3.2. Processing, morphology, and properties of SBS fibers

3.2.1. Processing and morphology of SBS fibers

Although the CL-1 blend fibers possessed decent conductivity, their mechanical properties were too poor to be further processed into any products for real applications. Additionally, the high PANI load (50 wt %) increased the fiber cost. To address these issues, the ratio of the blend solution was reduced by co-spinning it with a neat cellulose solution to engineer heterogeneous SBS fibers. This SBS structural design

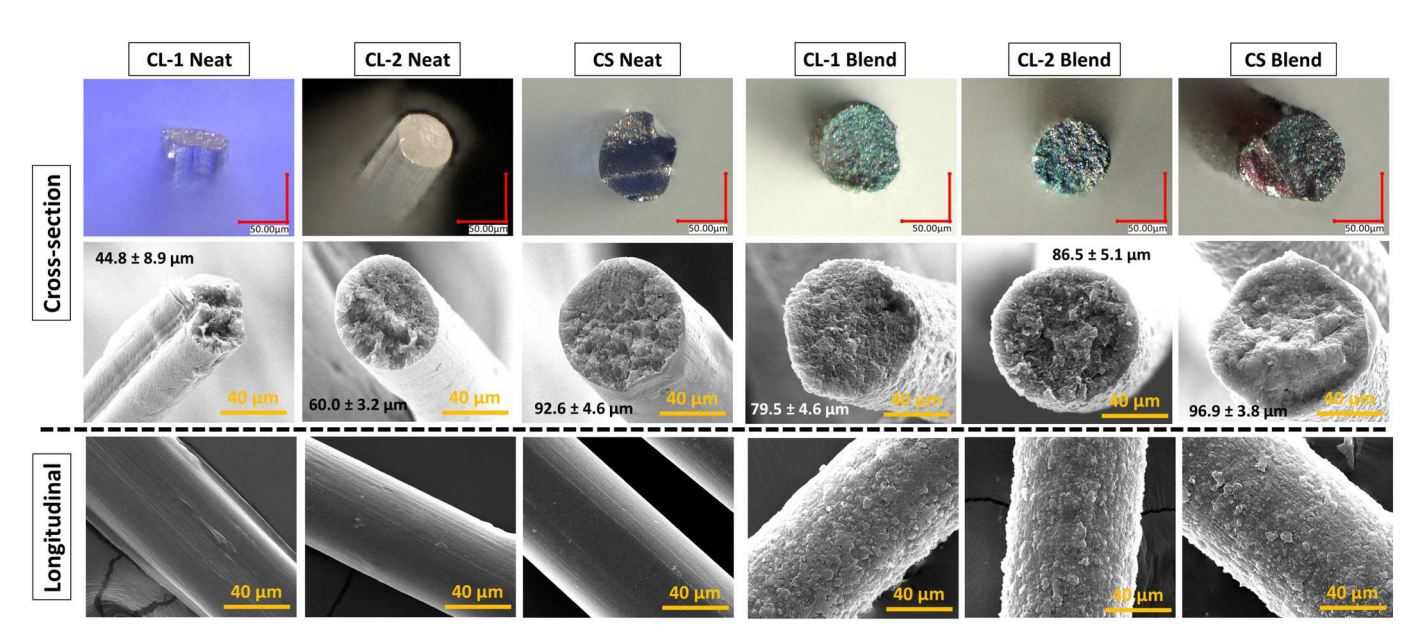


Fig. 1. Cross-sectional and longitudinal images of neat and blend monojet fibers. The inserted numbers indicate average fiber diameters.

Table 2Tensile properties and electrical conductivities of neat and blend as-spun fibers.

| Code | PANI loads (wt%) | Linear density (dtex) | Modulus (cN/dtex) | Tenacity (cN/dtex) | Elongation (%) | Conductivity (S/cm) |
|------------|------------------|-----------------------|-------------------|--------------------|----------------|----------------------------|
| CL-1 Neat | 0 | 24.8 ± 2.1 | 24.6 ± 3.5 | 0.83 ± 0.09 | 3.9–7.5 | $2.3 – 5.2 \times 10^{-9}$ |
| CL-2 Neat | 0 | 41.8 ± 1.3 | 23.1 ± 2.6 | 0.73 ± 0.07 | 13.9-28.2 | $0.6 – 1.2 \times 10^{-8}$ |
| CS Neat | 0 | 83.6 ± 1.5 | 21.6 ± 3.1 | 0.68 ± 0.07 | 9.8-19.4 | $2.0 – 5.1 \times 10^{-8}$ |
| CL-1 Blend | 50 | 55.2 ± 2.2 | 8.1 ± 1.3 | 0.17 ± 0.04 | 2.2-6.4 | $0.7 – 1.5 \times 10^{-2}$ |
| CL-2 Blend | 33.3 | 70.6 ± 2.9 | 19.3 ± 1.9 | 0.51 ± 0.07 | 4.4-12.8 | $2.2 – 5.5 \times 10^{-8}$ |
| CS Blend | 20 | 98.3 ± 3.0 | 19.6 ± 2.1 | 0.59 ± 0.07 | 4.9–11.2 | $1.3 4.4 \times 10^{-8}$ |

introduced the neat cellulose (CL-2 Neat or CS Neat) as a substrate to support the fragile PANI-riched blend with both components extruded as separated continuous phases except at the interface. Through the surface and cross-section morphologies of the fibers under SEM (Fig. 2), a clear SBS structure containing two phases was observed on all these fibers. The smooth transition from one phase to the other indicated great interfacial bondings. The surface of the neat side was smooth with a white (CL_SBS) or a blue (CS_SBS) color (Fig. 3). The blend side was relatively rough due to the PANI aggregates. These were consistent with the morphologies of their respective neat and blend fibers.

Although the processing conditions and the feeding ratio of the neat cellulose and cellulose/PANI blend for the two SBS fibers were the same, the two SBS fibers exhibited different morphologies. This was due to the

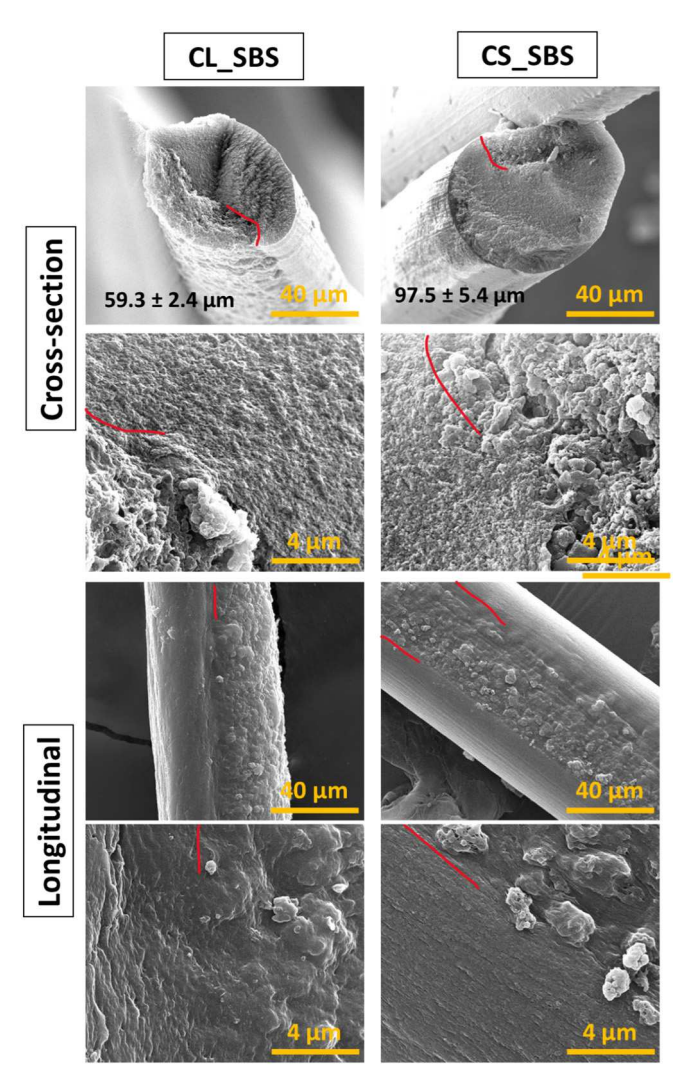


Fig. 2. SEM images of SBS as-spun fibers. The inserted numbers indicate average fiber diameters. The red lines are the speculated boundaries between the two phases.

solution flow instability originating from the viscosity difference between the two solutions during the SBS spinning. As can be seen in Fig. S2, all the dope solutions had proper viscosities falling into a spinnable range of 10^2 – 10^4 mPa·s as reported in the literature (Li et al., 2010; Liu, Liu, et al., 2019; Xie et al., 2021; Zhang et al., 2010). However, the viscosities of the two SBS solutions were different and the magnitude of the difference played a key role in determining the fiber interface and the cross-section morphology. Our previous study has shown that a large viscosity difference of more than two orders of magnitude can distort the fiber interface and generate an irregular fiber cross-section, sometimes resulting in poor mechanical properties (Liu et al., 2022). Here, the viscosity differences between the two SBS solutions were relatively small and therefore the solution flows inside and near the end of the spinneret were stable. At $50 \,\mathrm{s}^{-1}$, the viscosities of the solutions for CL_SBS were 1788 vs. 430 mPa·s and 796 vs. 430 mPa·s for CS_SBS. Fig. 3a & a' show pictures of stable solutions flowing inside the conical tip and liquid fibers that just entered the coagulation bath with clear linear boundaries between the two sides on the fiber surface. However, it was found that CL SBS and CS SBS presented different shapes of interfacial lines when examining the boundaries between the two components from the fiber internal via SEM images (Figs. 2 & 3). The CL SBS fiber showed a roughly side-by-side Janus architecture, and the blend side had a slightly concave shape; while the CS SBS fiber displayed an eccentric architecture that was similar to the spinning nozzle used. The blend side of CS SBS was convex as compared to the concave shape of CL-SBS. The schemes in Fig. 3a & a' illustrate the two flow dynamics that explain the formation of the fiber morphologies. When the two solutions are fed into the spinneret and meet in the conical tip, fluid with lower viscosity tends to encapsulate the fluid with higher viscosity governed by the Principle of Minimizing Energy Dissipation law. The low-viscosity fluid has a smaller friction against the pipe wall than the high-viscosity fluid, therefore, it tends to spread along the wall to surround the high-viscosity one (Borzacchiello, Leriche, Blottiere, & Guillet, 2014; Joseph, Nguyen, & Beavers, 1984; Kerswell, 2011; Liu et al., 2022; MacLean, 1973; Southern & Ballman, 1979; Uhland, 1977; White & Lee, 1975; Yue, Zhou, Dooley, & Feng, 2008). In this study, the viscosity of CS Neat was roughly $1.5 \times$ of that of CL-1 Blend at the same shear rate; while CL-2 Neat had a viscosity of approximately 3.4× of that of CL-1 Blend. A smaller viscosity difference resulted in less flow instability, which helped to maintain an eccentric geometry for CS SBS compared to the CL SBS fibers with a higher viscosity difference. This phenomenon can be utilized to tailor the surface areas of different components within the same fibers. For example, more PANI blend on the fiber surface will benefit chemical sensing-related applications. To achieve this, the viscosity of the neat solution can be increased by raising the cotton concentration to create a large viscosity difference. Theoretically, if the viscosity difference reaches a certain point, the SBS fibers will exhibit an encapsulating cross-sectional configuration (i.e., coresheath), maximizing the area of the low viscosity side on the fiber surface.

3.2.2. Mechanical and electrical properties of SBS fibers

Table 3 lists the linear density, tensile properties, and electrical conductivity of SBS as-spun fibers. Both SBS fibers had greatly improved mechanical properties approaching the level of their respective neat

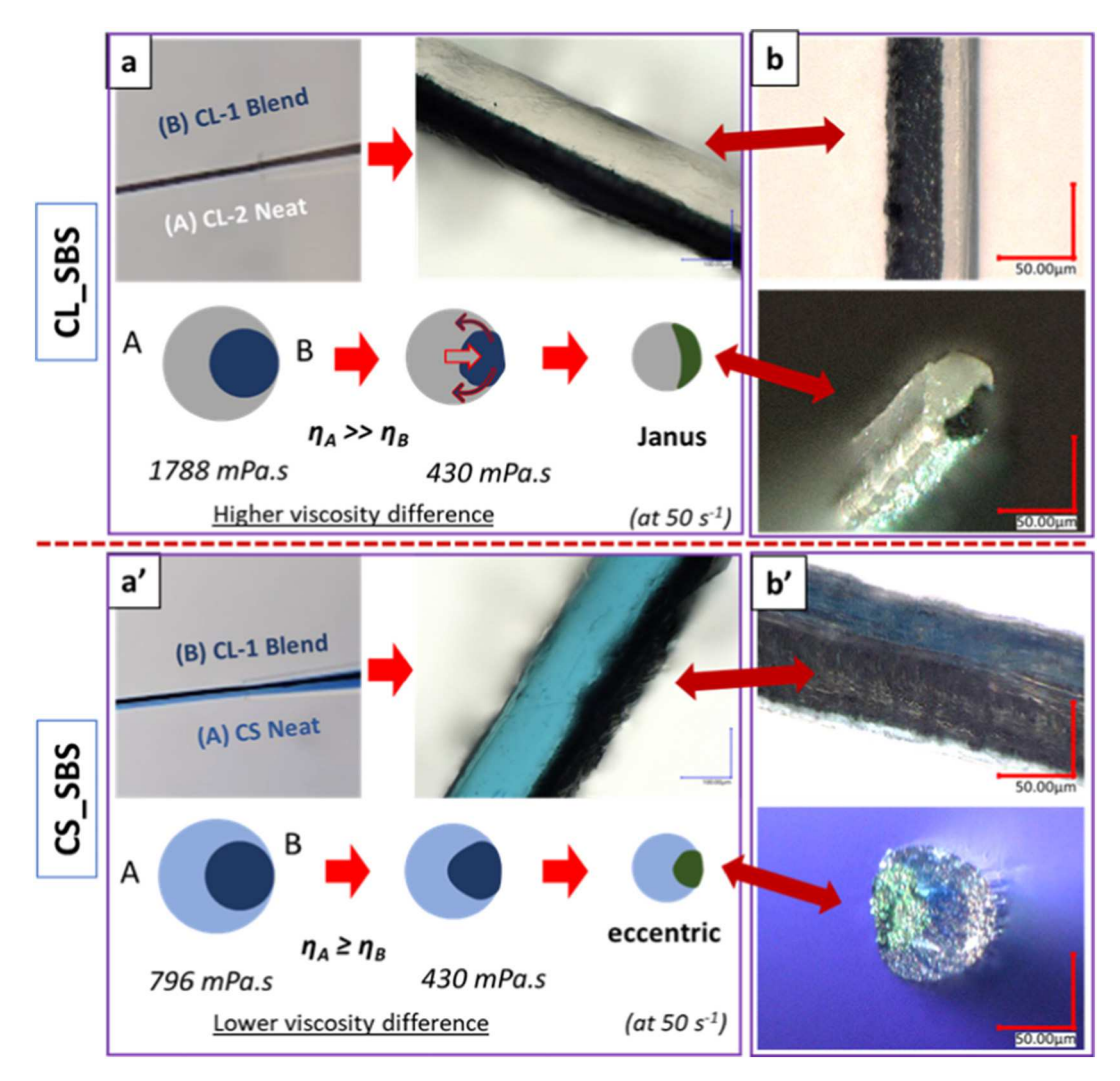


Fig. 3. (a & a') Illustration of SBS spinning, including the images of the polymer jets entering the coagulation bath and the evolution schemes of the fiber cross-sectional configurations. (b & b') Optical images of SBS fibers after coagulation.

Table 3Tensile properties and electrical conductivities of SBS as-spun fibers.

| Code | PANI loads (wt%) | Linear density (dtex) | Modulus (cN/dtex) | Tenacity (cN/dtex) | Elongation at break (%) | Conductivity (S/cm) |
|------------------|------------------|--------------------------------|---|---|-------------------------|---|
| CL_SBS CS_SBS | 12.5 7.1 | $41.3 \pm 1.7 \\ 84.6 \pm 2.3$ | $\begin{array}{c} 23.4 \pm 2.9 \\ 20.8 \pm 2.0 \end{array}$ | $\begin{array}{c} 0.65 \pm 0.06 \\ 0.62 \pm 0.07 \end{array}$ | 5.9–12.8 5.3–10.8 | $\begin{array}{c} 2.75.9 \times 10^{-3} \\ 1.33.5 \times 10^{-3} \end{array}$ |

fibers when compared to the blend fibers. For instance, the tensile tenacity of CS_SBS was 0.62 cN/dtex, slightly lower than that of CS Neat (0.68 cN/dtex), but much higher than CL-1 Blend (0.17 cN/dtex). However, the conductivities of both CL_SBS and CS_SBS were much higher than the monojet blend fibers. The conductivities of CL-SBS, CS_SBS, CL-1 Blend, CL_2 Blend, and CS_Blend were $2.7-5.9 \times 10^{-3}$, $1.3-3.5\times10^{-3}$, $0.68-1.5\times10^{-2}$, $2.2-5.5\times10^{-8}$, and $1.3-4.4\times10^{-8}$ in S/cm, respectively. The overall PANI loads (wt%) in these fibers were 12.5, 7.1, 50, 33, and 20 in the order listed above. These results demonstrated that fibers with the SBS structure could achieve high electrical conductance without applying high filler loads since fillers were distributed only on one side of the fiber to satisfy the percolation threshold instead of the whole fiber as in a blend. This is an important advantage in terms of cost since conductive fillers are generally more expensive than the conventional polymer matrix (recycled cotton wastes in this study). Additionally, it is expected that the overall mechanical and electrical properties of SBS fibers can be manipulated by adjusting the flow rate ratio of the two solutions in SBS spinning to engineer fibers for various applications. The flow rate ratio of the neat cellulose solution and the cellulose/PANI blend solution in this study was 3:1. Increasing the neat cellulose solution ratio should improve the mechanical properties further and increasing the blend solution ratio should alter sensing functions.

3.2.3. The influence of hot drawing on fiber tensile properties and conductivity

To enhance the cellulose molecular chain alignment and improve mechanical strength, both as-spun monojet fibers (neat and blend fibers) and SBS fibers were subject to drawing in hot water after the coagulation process. Given the unique SBS fiber structure, not only the mechanical properties of the drawn fibers were evaluated, but also their conductivity and the tensile fractures to examine the effect of drawing on the SBS fiber interface. None of the blend fibers (CL-1 Blend, CL-2 Blend, CS Blend) were able to be drawn. These fibers broke at very low drawing

ratios due to severe stress concentrations on the weak points where PANI aggregated. SBS fibers could be stretched up to a ratio of 1.32. The stress-strain curves in Fig. 4a demonstrated the increased tensile tenacity and decreased ductility of SBS fibers after hot drawing. The tenacity of CL_SBS-D (0.77 cN/dtex) increased 18.4 % from the as-spun fiber (0.65 cN/dtex) and was superior to that of CL-2 Neat (0.73 cN/dtex). Similarly, the tenacity of CS_SBS-D (0.72 cN/dtex) increased 11.6 % from the as-spun fiber (0.62 cN/dtex). The elongation at break for both fibers dropped 35.3 % and 24.2 %, respectively. The morphology of fibers after hot drawing was demonstrated in Fig. S3.

The tensile fracture images of SBS drawn fiber are shown in Fig. 4b. The fracture surfaces were rough and granular, resulting from the microfibril structures of cellulose fibers. There was no cracking, splitting, or shearing at the interface observed cross-sectionally and longitudinally, which indicated that the bondings between the two phases were strong, attributing to the sufficient mixing of the two components at the interface during fiber formation. At the same time, the mixing was only limited at the interface as observed in fiber cross-sectional images and suggested by the tensile results, as illustrated in Fig. 4c. Related to

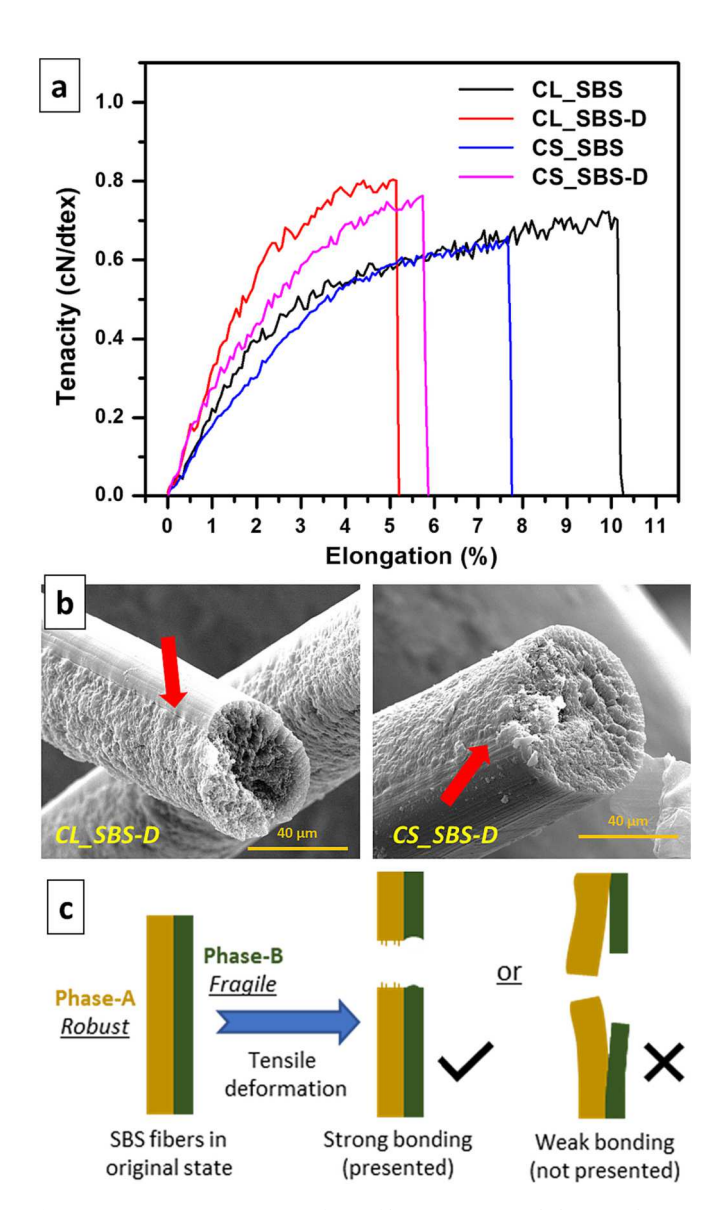


Fig. 4. (a) Stress-strain curves of SBS fibers (as-spun and drawn); (b) SEM images of the tensile fractured surface of SBS-drawn fibers (the red arrows mark the interface lines); (c) Deduced schematic models of the tensile failure of SBS fibers.

conductivity (Table S2), the drawn fibers had conductivities of 1.2–2.7 $\times~10^{-3}$ S/cm and 0.71–1.7 $\times~10^{-3}$ S/cm for CL_SBS-D and CS_SBS-D, respectively. The conductivities were slightly lower than those before drawing (2.7–5.9 $\times~10^{-3}$ for CL_SBS and 1.3–3.5 $\times~10^{-3}$ for CS_SBS). The results supported our hypothesis that neat cellulose effectively served as the substrate carrying the fragile cellulose/PANI blend phase, which provided electrical conductivity without negatively affecting the tensile strength of the fibers.

3.3. Fabricating SBS fibers into conductive yarns and chemical sensors

Based on their mechanical and conductive properties, the SBS fibers have great potential applications in various smart wearables. Two examples were demonstrated, i.e., twisting the SBS fibers into a conductive yarn and fabricating SBS fibers into a chemical sensor. The SBS fibers were flexible enough to be twisted with polyester fibers into a conductive yarn, which was strong and flexible enough to be knotted and its electrical resistance was approximately 50 Kohm. Fig. 5a shows that, when applied as the conductive wire of a circuit, 1.5 cm of the yarn could power an LED light (Fig. 5a).

Taking advantage of PANI's reversible redox reaction associated with doping and de-doping, PANI fibers can be utilized for sensing chemicals and gases. CL-1 Blend, CL-SBS D, and CS SBS D fibers were fabricated into sensors, and their performance toward ammonia (NH₃) gas sensing was evaluated using a customized device as shown in Fig. 5b. Approximately 50 fibers were installed in T/U-shaped electrodes connected to an electrometer (Keithley Agilent 34972A LXI and 34901A). The electrodes were placed in a chamber, which was vacuumed for 2 min before being filled with NH₃ gas (250 ppm) for 2 min or 5 min ("on" mode), and then flushed by dry air ("off" mode). The resistance of the sensor was monitored for 10 min. Results showed that all the samples rapidly responded to the influx of NH3 as reflected by the dramatically increased relative resistance in a few seconds as reported in the literature (Eising, Cava, Salvatierra, Zarbin, & Roman, 2017; Kumar, Rawal, Kaur, & Annapoorni, 2017; Tanguy et al., 2018; Zhang, Kim, Chen, Tuller, & Rutledge, 2014). The resistance kept increasing until NH₃ reached its highest concentration. After that, once NH3 was flushed with air, the fibers gained back their conductivity gradually. The CL-SBS-D fibers displayed better performance in terms of both sensing speed and sensitivity than CS_SBS-D. This can be explained by the larger amount of PANI that was exposed on the CL-SBS-D fiber surface as a result of the fiber morphology shown in Figs. 2 & 3. Surprisingly, CL-1 Blend did not perform better than the two SBS fibers, although it had the same PANI load (50 %) on the sensing phase (i.e., PANI-containing phase) as those SBS fibers but a much large surface area. This may indicate that more PANI particles were embedded in the fiber core. The sensing results further testified to the advantages of the SBS structure in PANI-based fiber production.

4. Conclusion

In this work, eco-friendly alkali/urea solvents were used to dissolve cotton waste and produce multi-functional cellulose-based composite fibers for wearable e-textile applications. Biocompatible PANI was applied as the conductive filler. In order to obtain fibers with both desirable conductivity and enhanced mechanical properties, a modified wet-spinning process to engineer the composite fibers with two cocontinuous heterogeneous phases arranged in an SBS architecture was developed. One phase of the SBS fibers was neat cellulose, which provided processability and mechanical property for the fibers; the other phase was a high load of PANI (50 wt%) blended in cellulose solutions that provided functionality. The resulting SBS fibers had lower overall PANI load (only 7.1 wt% and 12.5 wt%) which helped reduce costs while maintaining decent conductivities. After hot-drawing, SBS-drawn fibers gained improved mechanical properties. The SBS fibers showed two distinct phases by examining the surface and cross-sectional

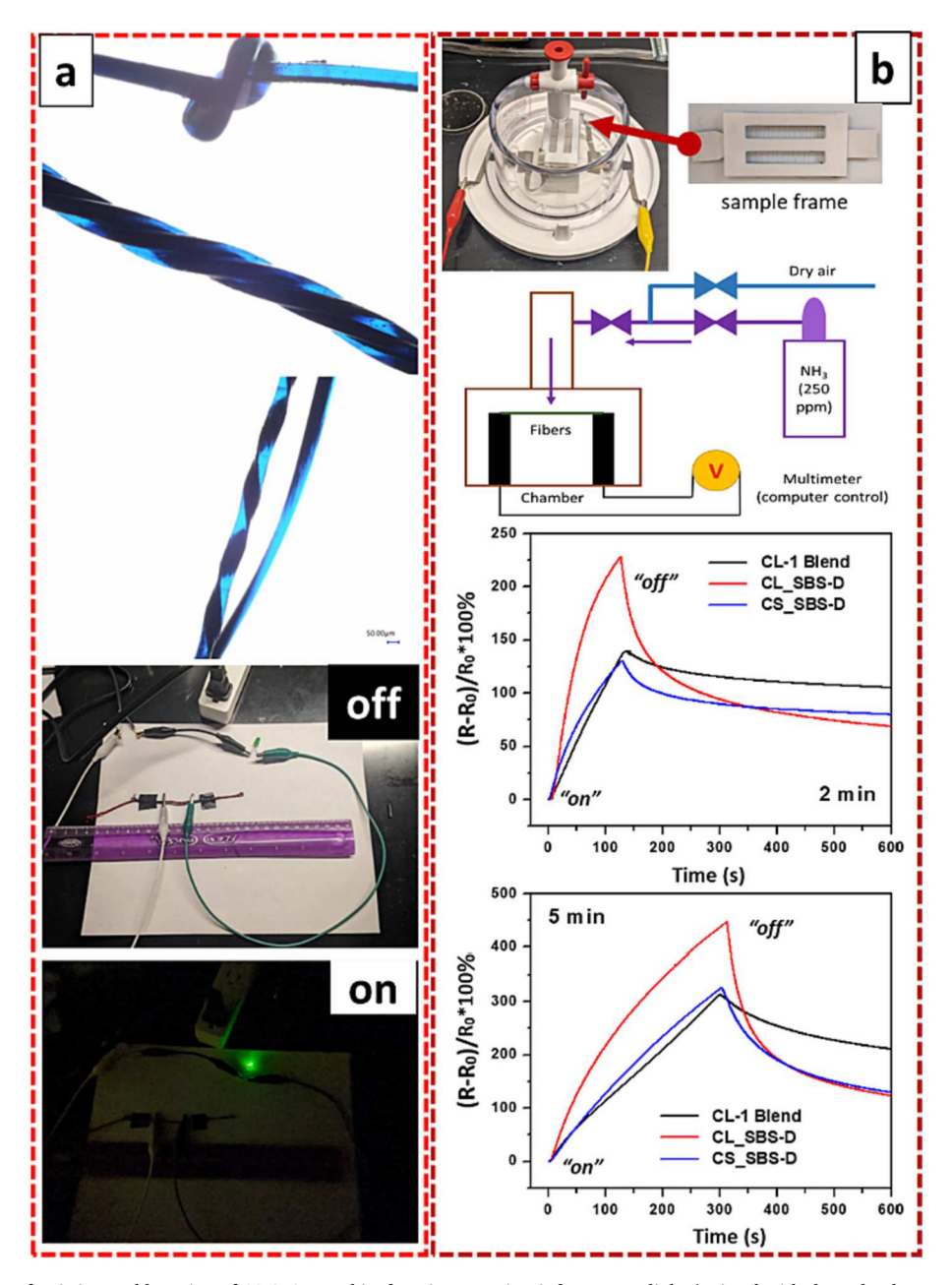


Fig. 5. (a) Demonstration of twisting and knotting of CS_SBS-D and its function as a circuit for an LED light (twisted with the red polyester yarns); (b) The setting of NH_3 sensing experiment (top) and the relative resistance $(R-R_0)/R_0$ of fiber samples in two different testing modes (bottom).

morphologies and demonstrated strong interfacial bondings between the two phases as evidenced by the tensile fractures. With decent strength, flexibility, and conductivities, the SBS-drawn fibers could be twisted into yarns and function in a circuit to power an LED light. They were also fabricated into a smart sensor for hazardous NH₃ gas detection. Overall, this study demonstrated a new processing technique to manufacture cellulose-based multi-functional fibers for smart e-textiles.

Disclaimer

Any opinions, findings, and conclusions or recommendations expressed in this material are those of the author(s) and do not necessarily reflect the views of the National Science Foundation.

CRediT authorship contribution statement

Wangcheng Liu: Formal analysis, Investigation, Methodology,

Writing – original draft, Writing – review & editing. Hang Liu: Conceptualization, Funding acquisition, Project administration, Supervision, Writing – review & editing. Zihui Zhao: Investigation. Dan Liang: Investigation. Wei-Hong Zhong: Writing – review & editing. Jinwen Zhang: Supervision.

Declaration of competing interest

Hang Liu reports financial support was provided by National Science Foundation. Hang Liu reports financial support was provided by Walmart Foundation.

Data availability

Data will be made available on request.

Acknowledgment

Wangcheng Liu is a Washington Research Foundation Postdoctoral Fellow

This material is based upon work supported by the National Science Foundation under Grant 2145468 and Walmart Foundation Project 130813.

We would also like to express our gratitude to the Franceschi Microscopy and Imaging Center (FMIC) at Washington State University for the use of SEM.

Appendix A. Supplementary data

Supplementary data to this article can be found online at $\frac{https:}{doi.}$ org/10.1016/j.carbpol.2023.121308.

References

- Balint, R., Cassidy, N. J., & Cartmell, S. H. (2014). Conductive polymers: Towards a smart biomaterial for tissue engineering. *Acta Biomaterialia*, 10(6), 2341–2353.
- Bavatharani, C., Muthusankar, E., Wabaidur, S. M., Alothman, Z. A., Alsheetan, K. M., Mana Al-Anazy, M., & Ragupathy, D. (2021). Electrospinning technique for production of polyaniline nanocomposites/nanofibres for multi-functional applications: A review. Synthetic Metals, 271, Article 116609.
- Bhadra, S., Khastgir, D., Singha, N. K., & Lee, J. H. (2009). Progress in preparation, processing and applications of polyaniline. *Progress in Polymer Science*, 34(8), 783–810.
- Borzacchiello, D., Leriche, E., Blottiere, B., & Guillet, J. (2014). On the mechanism of viscoelastic encapsulation of fluid layers in polymer coextrusion. *Journal of Rheology*, 58(2), 493–512.
- Cai, J., & Zhang, L. (2005). Rapid dissolution of cellulose in LiOH/urea and NaOH/urea aqueous solutions. *Macromolecular Bioscience*, 5(6), 539–548.
- Cai, J., & Zhang, L. (2006). Unique gelation behavior of cellulose in NaOH/urea aqueous solution. *Biomacromolecules*, 7(1), 183–189.
- Cai, J., Zhang, L., Zhou, J., Li, H., Chen, H., & Jin, H. (2004). Novel fibers prepared from cellulose in NaOH/urea aqueous solution. *Macromolecular Rapid Communications*, 25 (17), 1558–1562.
- Castano, L. M., & Flatau, A. B. (2014). Smart fabric sensors and e-textile technologies: a review. Smart Materials and Structures, 23(5), Article 053001.
- Chen, J., Guan, Y., Wang, K., Zhang, X., Xu, F., & Sun, R. (2015). Combined effects of raw materials and solvent systems on the preparation and properties of regenerated cellulose fibers. *Carbohydrate Polymers*, 128, 147–153.
- Chen, X., Burger, C., Wan, F., Zhang, J., Rong, L., Hsiao, B. S., ... Zhang, L. (2007). Structure study of cellulose fibers wet-spun from environmentally friendly NaOH/urea aqueous solutions. *Biomacromolecules*, 8(6), 1918–1926.
- Ćirić-Marjanović, G. (2013). Recent advances in polyaniline research: Polymerization mechanisms, structural aspects, properties and applications. Synthetic Metals, 177, 1–47.
- Eising, M., Cava, C. E., Salvatierra, R. V., Zarbin, A. J. G., & Roman, L. S. (2017). Doping effect on self-assembled films of polyaniline and carbon nanotube applied as ammonia gas sensor. Sensors and Actuators B: Chemical, 245, 25–33.
- Grancarić, A. M., Jerković, I., Koncar, V., Cochrane, C., Kelly, F. M., Soulat, D., & Legrand, X. (2018). Conductive polymers for smart textile applications. *Journal of Industrial Textiles*, 48(3), 612–642.
- Guo, B., & Ma, P. X. (2018). Conducting polymers for tissue engineering. Biomacromolecules, 19(6), 1764–1782.
- Härdelin, L., & Hagström, B. (2015). Wet spun fibers from solutions of cellulose in an ionic liquid with suspended carbon nanoparticles. *Journal of Applied Polymer Science*, 132(6), 41417.
- He, H., Zhang, L., Guan, X., Cheng, H., Liu, X., Yu, S., ... Ouyang, J. (2019). Biocompatible conductive polymers with high conductivity and high stretchability. ACS Applied Materials & Interfaces, 11(29), 26185–26193.
- Hu, J., Meng, H., Li, G., & Ibekwe, S. I. (2012). A review of stimuli-responsive polymers for smart textile applications. Smart Materials and Structures, 21(5), Article 053001.
- Ismar, E., Kurşun Bahadir, S., Kalaoglu, F., & Koncar, V. (2020). Futuristic clothes: Electronic textiles and wearable technologies. Global Challenges, 4(7), 1900092.
- Jia, G., Wang, H., Yan, L., Wang, X., Pei, R., Yan, T., ... Guo, X. (2005). Cytotoxicity of carbon nanomaterials: Single-wall nanotube, multi-wall nanotube, and fullerene. *Environmental Science & Technology*, 39(5), 1378–1383.
- Joseph, D., Nguyen, K., & Beavers, G. (1984). Non-uniqueness and stability of the configuration of flow of immiscible fluids with different viscosities. *Journal of Fluid Mechanics*, 141, 319–345.
- Kerswell, R. (2011). Exchange flow of two immiscible fluids and the principle of maximum flux. *Journal of Fluid Mechanics*, 682, 132–159.
- Kim, D. H., Park, S. Y., Kim, J., & Park, M. (2010). Preparation and properties of the single-walled carbon nanotube/cellulose nanocomposites using Nmethylmorpholine-N-oxide monohydrate. *Journal of Applied Polymer Science*, 117(6), 3588–3594.
- Kim, H.-S., Hobbs, H. L., Wang, L., Rutten, M. J., & Wamser, C. C. (2009). Biocompatible composites of polyaniline nanofibers and collagen. Synthetic Metals, 159(13), 1313–1318.

- Kumar, L., Rawal, I., Kaur, A., & Annapoorni, S. (2017). Flexible room temperature ammonia sensor based on polyaniline. Sensors and Actuators B: Chemical, 240, 408–416.
- Lai, J., Yi, Y., Zhu, P., Shen, J., Wu, K., Zhang, L., & Liu, J. (2016). Polyaniline-based glucose biosensor: A review. *Journal of Electroanalytical Chemistry*, 782, 138–153.
- Li, R., Chang, C., Zhou, J., Zhang, L., Gu, W., Li, C., ... Kuga, S. (2010). Primarily industrialized trial of novel fibers spun from cellulose dope in NaOH/urea aqueous solution. *Industrial & Engineering Chemistry Research*, 49(22), 11380–11384.
- Li, R., Wang, S., Lu, A., & Zhang, L. (2015). Dissolution of cellulose from different sources in an NaOH/urea aqueous system at low temperature. *Cellulose*, 22(1), 339–349.
- Liu, W., Chang, Y.-C., Zhang, J., & Liu, H. (2022). Wet-spun side-by-side electrically conductive composite fibers. ACS Applied Electronic Materials, 4(4), 1979–1988.
- Liu, W., Liu, S., Liu, T., Liu, T., Zhang, J., & Liu, H. (2019). Eco-friendly post-consumer cotton waste recycling for regenerated cellulose fibers. *Carbohydrate Polymers*, 206, 141–148.
- Liu, W., Zhong, T., Liu, T., Zhang, J., & Liu, H. (2020). Preparation and characterization of electrospun conductive janus nanofibers with polyaniline. ACS Applied Polymer Materials, 2(7), 2819–2829.
- Liu, Y., Wang, Y., Nie, Y., Wang, C., Ji, X., Zhou, L., ... Zhang, S. (2019). Preparation of MWCNTs-graphene-cellulose fiber with ionic liquids. ACS Sustainable Chemistry & Engineering, 7(24), 20013–20021.
- Low, K., Chartuprayoon, N., Echeverria, C., Li, C., Bosze, W., Myung, N. V., & Nam, J. (2014). Polyaniline/poly (ε-caprolactone) composite electrospun nanofiber-based gas sensors: Optimization of sensing properties by dopants and doping concentration. *Nanotechnology*, 25(11), Article 115501.
- Low, K., Horner, C. B., Li, C., Ico, G., Bosze, W., Myung, N. V., & Nam, J. (2015). Composition-dependent sensing mechanism of electrospun conductive polymer composite nanofibers. Sensors and Actuators B: Chemical, 207, 235–242.
- Lu, J., Zhang, H., Jian, Y., Shao, H., & Hu, X. (2012). Properties and structure of MWNTs/cellulose composite fibers prepared by Lyocell process. *Journal of Applied Polymer Science*, 123(2), 956–961.
- Ma, J., Pu, H., He, P., Zhao, Q., Pan, S., Wang, Y., & Wang, C. (2021). Robust cellulosecarbon nanotube conductive fibers for electrical heating and humidity sensing. *Cellulose*, 28(12), 7877–7891.
- MacLean, D. L. (1973). A theoretical analysis of bicomponent flow and the problem of interface shape. Transactions of the Society of Rheology, 17(3), 385–399.
- Mahmoudian, S., Reza Sazegar, M., Afshari, N., & Uzir Wahit, M. (2017). Graphene reinforced regenerated cellulose nanocomposite fibers prepared by lyocell process. *Polymer Composites*, 38, E81–E88.
- Mao, Y., Zhang, L., Cai, J., Zhou, J., & Kondo, T. (2008). Effects of coagulation conditions on properties of multifilament fibers based on dissolution of cellulose in NaOH/urea aqueous solution. *Industrial & Engineering Chemistry Research*, 47(22), 8676–8683.
- Mirabedini, A., Foroughi, J., & Wallace, G. G. J. R.a. (2016). Developments in conducting polymer fibres: from established spinning methods toward advanced applications. 6 (50), 44687–44716.
- Norris, I. D., Shaker, M. M., Ko, F. K., & MacDiarmid, A. G. (2000). Electrostatic fabrication of ultrafine conducting fibers: Polyaniline/polyethylene oxide blends. Synthetic Metals, 114(2), 109–114.
- Patel, S., Park, H., Bonato, P., Chan, L., & Rodgers, M. (2012). A review of wearable sensors and systems with application in rehabilitation. *Journal of Neuroengineering* and Rehabilitation, 9(1), 1–17.
- Qi, H., Chang, C., & Zhang, L. (2008). Effects of temperature and molecular weight on dissolution of cellulose in NaOH/urea aqueous solution. *Cellulose*, 15(6), 779–787. Qi, H., Schulz, B.r., Vad, T., Liu, J., Mäder, E., Seide, G., & Gries, T. (2015). Novel carbon
- Qi, H., Schulz, B.r., Vad, T., Liu, J., Mader, E., Seide, G., & Gries, T. (2015). Novel carbon nanotube/cellulose composite fibers as multi-functional materials. ACS Applied Materials & Interfaces, 7(40), 22404–22412.
- Qiu, C., Zhu, K., Zhou, X., Luo, L., Zeng, J., Huang, R., ... Zhang, L. (2018). Influences of coagulation conditions on the structure and properties of regenerated cellulose filaments via wet-spinning in LiOH/urea solvent. ACS Sustainable Chemistry & Engineering, 6(3), 4056–4067.
- Rahatekar, S. S., Rasheed, A., Jain, R., Zammarano, M., Koziol, K. K., Windle, A. H., ... Kumar, S. (2009). Solution spinning of cellulose carbon nanotube composites using room temperature ionic liquids. *Polymer*, 50(19), 4577–4583.
- Rose, M., & Palkovits, R. (2011). Cellulose-based sustainable polymers: State of the art and future trends. *Macromolecular Rapid Communications*, 32(17), 1299–1311.
- Sayyed, A. J., Deshmukh, N. A., & Pinjari, D. V. (2019). A critical review of manufacturing processes used in regenerated cellulosic fibres: Viscose, cellulose acetate, cuprammonium, LiCl/DMAc, ionic liquids, and NMMO based lyocell. *Cellulose*, 26(5), 2913–2940.
- Sen, T., Mishra, S., & Shimpi, N. G. (2016). Synthesis and sensing applications of polyaniline nanocomposites: A review. RSC Advances, 6(48), 42196–42222.
- Shi, J., Liu, S., Zhang, L., Yang, B., Shu, L., Yang, Y., ... Chen, W. (2020). Smart textile-integrated microelectronic systems for wearable applications. Advanced Materials, 32 (5), 1901958.
- Shi, Q., Sun, J., Hou, C., Li, Y., Zhang, Q., & Wang, H. (2019). Advanced functional fiber and smart textile. Advanced Fiber Materials, 1(1), 3–31.
- Sousa, S. P., Peixoto, T., Santos, R. M., Lopes, A., Paiva, M.d. C., & Marques, A. T. (2020). Health and safety concerns related to CNT and graphene products, and related composites. *Journal of Composites Science*, 4(3), 106.
- Southern, J. H., & Ballman, R. L. (1979). Preferential wetting phenomenon in bicomponent polymer melt flow. *Journal of Applied Polymer Science*, 24(3), 693–701.
- Stoppa, M., & Chiolerio, A. (2014). Wearable electronics and smart textiles: a critical review. sensors, 14(7), 11957–11992.
- Tanguy, N. R., Thompson, M., & Yan, N. (2018). A review on advances in application of polyaniline for ammonia detection. Sensors and Actuators B: Chemical, 257, 1044–1064.

- Tu, H., Xie, K., Ying, D., Luo, L., Liu, X., Chen, F., ... Zhang, L. (2020). Green and economical strategy for spinning robust cellulose filaments. ACS Sustainable Chemistry & Engineering, 8(39), 14927–14937.
- Ucar, N., Kizildag, N., Onen, A., Karacan, I., & Eren, O. (2015). Polyacrylonitrile-polyaniline composite nanofiber webs: Effects of solvents, redoping process and dispersion technique. Fibers and Polymers, 16, 2223–2236.
- Uhland, E. (1977). Stratified two-phase flog of molten polymers in circular dies. Polymer Engineering & Science, 17(9), 671–681.
- Vehviläinen, M., Kamppuri, T., Rom, M., Janicki, J., Ciechańska, D., Grönqvist, S., ... Nousiainen, P. (2008). Effect of wet spinning parameters on the properties of novel cellulosic fibres. *Cellulose*, 15(5), 671–680.
- Wang, S., Lu, A., & Zhang, L. (2016). Recent advances in regenerated cellulose materials. Progress in Polymer Science, 53, 169–206.
- White, J. L., & Lee, B. L. (1975). Theory of interface distortion in stratified two-phase flow. Transactions of the Society of Rheology, 19(3), 457–479.
- Wick, P., Manser, P., Limbach, L. K., Dettlaff-Weglikowska, U., Krumeich, F., Roth, S., ... Bruinink, A. (2007). The degree and kind of agglomeration affect carbon nanotube cytotoxicity. *Toxicology Letters*, 168(2), 121–131.
- Xie, K., Tu, H., Dou, Z., Liu, D., Wu, K., Liu, Y., ... Fu, Q. (2021). The effect of cellulose molecular weight on internal structure and properties of regenerated cellulose fibers as spun from the alkali/urea aqueous system. *Polymer*, 215, Article 123379.
- Yang, K., Li, Y., Tan, X., Peng, R., & Liu, Z. (2013). Behavior and toxicity of graphene and its functionalized derivatives in biological systems. Small, 9(9–10), 1492–1503.

- Yang, T., Xie, D., Li, Z., & Zhu, H. (2017). Recent advances in wearable tactile sensors: Materials, sensing mechanisms, and device performance. *Materials Science and Engineering: R: Reports*, 115, 1–37.
- Yang, Y., Zhang, Y., Lang, Y., & Yu, M. (2018). Structure development in the condensed state of cellulose fiber regenerated from alkali complex solution. *Cellulose*, 25(3), 1555–1569.
- Yue, P., Zhou, C., Dooley, J., & Feng, J. J. (2008). Elastic encapsulation in bicomponent stratified flow of viscoelastic fluids. *Journal of Rheology*, 52(4), 1027–1042.
- Zeng, W., Shu, L., Li, Q., Chen, S., Wang, F., & Tao, X. M. (2014). Fiber-based wearable electronics: a review of materials, fabrication, devices, and applications. *Advanced Materials*, 26(31), 5310–5336.
- Zhang, H., Wang, Z., Zhang, Z., Wu, J., Zhang, J., & He, J. (2007). Regenerated-cellulose/multiwalled-carbon-nanotube composite fibers with enhanced mechanical properties prepared with the ionic liquid 1-allyl-3-methylimidazolium chloride. Advanced Materials, 19(5), 698–704.
- Zhang, S., Li, F.-X., Yu, J.-Y., & Hsieh, Y.-L. (2010). Dissolution behaviour and solubility of cellulose in NaOH complex solution. Carbohydrate Polymers, 81(3), 668–674.
- Zhang, Y., Kim, J. J., Chen, D., Tuller, H. L., & Rutledge, G. C. (2014). Electrospun polyaniline fibers as highly sensitive room temperature chemiresistive sensors for ammonia and nitrogen dioxide gases. Advanced Functional Materials, 24(25), 4005–4014.
- Zhu, K., Qiu, C., Lu, A., Luo, L., Guo, J., Cong, H., ... Wang, H. (2018). Mechanically strong multifilament fibers spun from cellulose solution via inducing formation of nanofibers. ACS Sustainable Chemistry & Engineering, 6(4), 5314–5321.